

# DETECTION OF NEGATIVE EFFECTIVE MAGNETIC PRESSURE INSTABILITY IN TURBULENCE SIMULATIONS

AXEL BRANDENBURG<sup>1,2</sup>, KOEN KEMEL<sup>1,2</sup>, NATHAN KLEEORIN<sup>3</sup>, DHRUBADITYA MITRA<sup>1</sup>, AND IGOR ROGACHEVSKII<sup>3</sup>

<sup>1</sup>NORDITA, AlbaNova University Center, Roslagstullsbacken 23, SE-10691 Stockholm, Sweden

<sup>2</sup>Department of Astronomy, AlbaNova University Center, Stockholm University, SE-10691 Stockholm, Sweden

<sup>3</sup>Department of Mechanical Engineering, Ben-Gurion University of the Negev, POB 653, Beer-Sheva 84105, Israel

(Dated: Revision: 1.83 )

Draft version December 3, 2024

## ABSTRACT

We present the first numerical demonstration of the negative effective magnetic pressure instability in direct numerical simulations of stably-stratified, externally-forced, isothermal hydromagnetic turbulence. By the action of this instability, initially uniform horizontal magnetic field forms flux concentrations whose scale is large compared to the turbulent scale. We further show that the magnetic energy of these large-scale structures is only weakly dependent on the magnetic Reynolds number. Our results supports earlier mean-field calculations and analytic work which identified this instability. Applications to the formation of active regions in the Sun are discussed.

*Subject headings:* MHD – Sun: dynamo – sunspots – turbulence

## 1. INTRODUCTION

The solar convection zone is highly turbulent and mixing is therefore expected to be efficient. Nevertheless, the Sun displays coherent structures encompassing several turbulent eddy scales. A well-known example is the large-scale magnetic field of the Sun that is antisymmetric about the equator and shows the 11 year solar cycle (Stenflo & Vogel 1986). Another prominent example in the Sun is the emergence of active regions and active longitudes. There is no universally accepted theory for this phenomenon. A commonly expressed conjecture involves non-axisymmetric modes of the solar dynamo (see, e.g., Jiang & Wang 2007).

A powerful tool for understanding the emergence of such large-scale structures from a turbulent background is mean-field dynamo theory (Moffatt 1978; Parker 1979; Krause & Rädler 1980). With the advent of powerful computers and numerical simulation tools, it has become possible to confront many of the mean-field predictions with simulations (Brandenburg & Subramanian 2005). Here we consider the idea that statistically steady, stratified, hydromagnetic turbulence with an initially uniform magnetic field is unstable to the Negative Effective Magnetic Pressure Instability (NEMPI). This instability is caused by the suppression of turbulent hydromagnetic pressure (isotropic part of combined Reynolds and Maxwell stresses) by the mean magnetic field. Under certain conditions (Kleeorin et al. 1990; Rogachevskii & Kleeorin 2007), this turbulent contribution can become so large that the effective mean magnetic pressure appears negative. This results in the excitation of NEMPI that causes formation of large-scale inhomogeneous magnetic structures. NEMPI as a large-scale instability of a turbulent state is similar to the large-scale dynamo instability that can be identified with the linear instability of the underlying mean-field dynamo equations. However, NEMPI does not increase the total magnetic flux, but it only redistributes it, creating large-scale concentrated magnetic flux regions at the expense of turbulent kinetic energy.

The magnetic suppression of the Reynolds stress was first found by Rädler (1974) and Rüdiger (1974). Considering also the Maxwell stress, Rüdiger et al. (1986) found that the mean effective magnetic tension can be suppressed by mean fields.

However, these calculations were based on the first-order smoothing approximation which is only valid at low fluid and magnetic Reynolds numbers. Kleeorin et al. (1990, 1996) considered the combined Reynolds and Maxwell stresses at large Reynolds numbers and found a sign reversal of the effective mean magnetic pressure. This result was based on the  $\tau$  approximation, but it has also been corroborated using the renormalization procedure (Kleeorin & Rogachevskii 1994).

The magnetic suppression of the combined Reynolds and Maxwell stresses is quantified in terms of new turbulent mean-field coefficients that relate the components of the sum of Reynolds and Maxwell stresses to the mean magnetic field. These coefficients depend on the magnetic field and have now been determined in direct numerical simulations (DNS) for a broad range of different cases, including unstratified forced turbulence (Brandenburg et al. 2010), isothermally stratified forced turbulence (Brandenburg et al. 2011), and turbulent convection (Käpylä et al. 2011). These simulations have clearly demonstrated that the mean effective magnetic pressure is negative for magnetic field strengths below about half the equipartition field strength. However, these DNS studies had not found the actual instability.

With a quantitative parameterization in place, it became possible to build mean-field models of stratified turbulence which clearly demonstrate NEMPI. In view of applications to the formation of active regions in the Sun, such simulations were originally done for an adiabatically stratified layer (Brandenburg et al. 2010). In addition, mean-field studies showed the existence of NEMPI even for isothermal stably stratified layers (Brandenburg et al. 2011; Kemel et al. 2011). This last result turned out to be important because it paved the way for this paper where we demonstrate NEMPI through DNS. Once the physical reality of this effect has been established, it will become important to apply it to real models of the Sun with proper boundary conditions and realistic stratification with convective flux and radiation transport. However, at this stage it is essential to isolate NEMPI as a physical effect under conditions that are as simple as possible.

## 2. THE MODEL

We consider a domain of size  $L_x \times L_y \times L_z$  in Cartesian coordinates,  $(x, y, z)$ , with periodic boundary conditions in

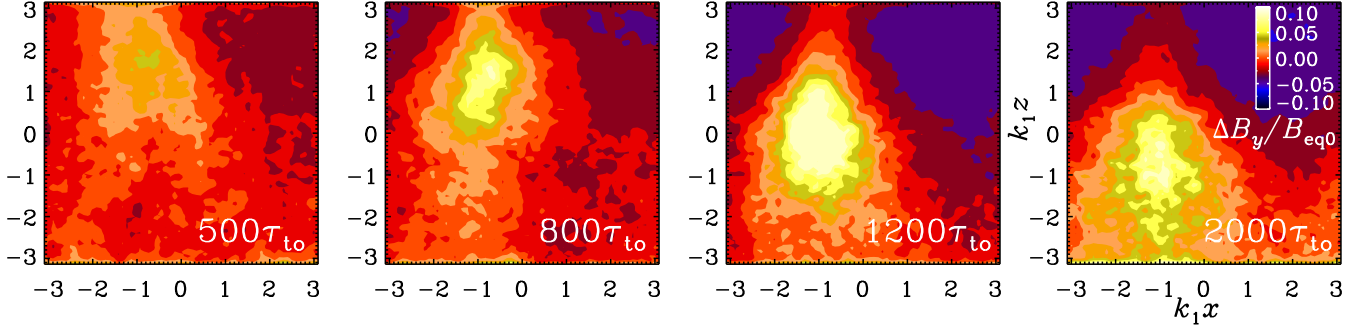


FIG. 1.—  $\Delta\bar{B}_y/B_{\text{eq}0}$  in the  $xz$  plane for  $\text{Re}_M = 6$  and  $B_0/B_{\text{eq}0} = 0.05$ , showing the ‘Potato sack’ effect. Time is in units of  $\tau_{\text{to}}$  (lower right corner).

the  $x$  and  $y$  directions and stress-free perfectly conducting boundaries at top and bottom ( $z = \pm L_z/2$ ). The volume-averaged density is therefore constant and equal to its initial value,  $\rho_0 = \langle \rho \rangle$ . We solve the equations for the velocity  $\mathbf{U}$ , the magnetic vector potential  $\mathbf{A}$ , and the density  $\rho$ ,

$$\rho \frac{D\mathbf{U}}{Dt} = \mathbf{J} \times \mathbf{B} - c_s^2 \nabla \rho + \nabla \cdot (2\nu \rho \mathbf{S}) + \rho(\mathbf{f} + \mathbf{g}), \quad (1)$$

$$\frac{\partial \mathbf{A}}{\partial t} = \mathbf{U} \times \mathbf{B} + \eta \nabla^2 \mathbf{A}, \quad (2)$$

$$\frac{\partial \rho}{\partial t} = -\nabla \cdot \rho \mathbf{U}, \quad (3)$$

where  $\nu$  and  $\eta$  are kinematic viscosity and magnetic diffusivity, respectively,  $\mathbf{B} = \mathbf{B}_0 + \nabla \times \mathbf{A}$  is the magnetic field consisting of a uniform part,  $\mathbf{B}_0 = (0, B_0, 0)$ , and a nonuniform part that is represented in terms of the magnetic vector potential  $\mathbf{A}$ ,  $\mathbf{J} = \nabla \times \mathbf{B}/\mu_0$  is the current density, and  $S_{ij} = \frac{1}{2}(U_{i,j} + U_{j,i}) - \frac{1}{3}\delta_{ij}\nabla \cdot \mathbf{U}$  is the traceless rate of strain tensor, where commas denote partial differentiation. The turbulence is driven with a forcing function  $\mathbf{f}$  that consists of random plane non-polarized waves with an average wavenumber  $k_f = 15 k_1$ , where  $k_1 = 2\pi/L_z$  is the lowest wavenumber in the domain. The forcing strength is such that the turbulent rms velocity is approximately independent of  $z$  with  $u_{\text{rms}} = \langle \mathbf{u}^2 \rangle^{1/2} \approx 0.1 c_s$ . The gravitational acceleration  $\mathbf{g} = (0, 0, -g)$  is chosen such that  $k_1 H_\rho = 1$ , which leads to a density contrast between bottom and top of  $\exp(2\pi) \approx 535$ . Here,  $H_\rho = c_s^2/g$  is the density scale height.

Our simulations are characterized by several non-dimensional parameters. We define the Reynolds number as  $\text{Re} = u_{\text{rms}}/\nu k_f$  and the magnetic Prandtl number as  $\text{Pr}_M = \nu/\eta$ . Following earlier work (Brandenburg et al. 2011), we consider values of  $\text{Pr}_M$  below unity and use  $\text{Pr}_M = 0.5$ . We consider values of  $\text{Re}_M$  varying in the range from 0.7 to 80. The magnetic field is expressed in units of the local equipartition field strength near the top,  $B_{\text{eq}} = \sqrt{\mu_0 \rho_0} u_{\text{rms}}$ , while the imposed field  $B_0$  is specified in units of the averaged value,  $B_{\text{eq}0} = \sqrt{\mu_0 \rho_0} u_{\text{rms}}$ . We monitor  $\Delta\bar{B}_y = \bar{B}_y - B_0$ , where  $\bar{B}_y$  is an average over  $y$  and a time interval  $\Delta t$  of about 10 eddy turnover times,  $\tau_{\text{to}} = (u_{\text{rms}} k_f)^{-1}$ . Occasionally, we also consider the turbulent-diffusive time scale,  $\tau_{\text{td}} = (\eta_{\text{to}} k_1^2)^{-1}$ , where  $\eta_{\text{to}} = u_{\text{rms}}/3k_f$  is the estimated turbulent magnetic diffusivity. Another diagnostic quantity is the rms magnetic field in the  $k = k_1$  Fourier mode,  $B_1$ , which is here taken as an average over  $2 \leq k_1 z \leq 3$ , which is close

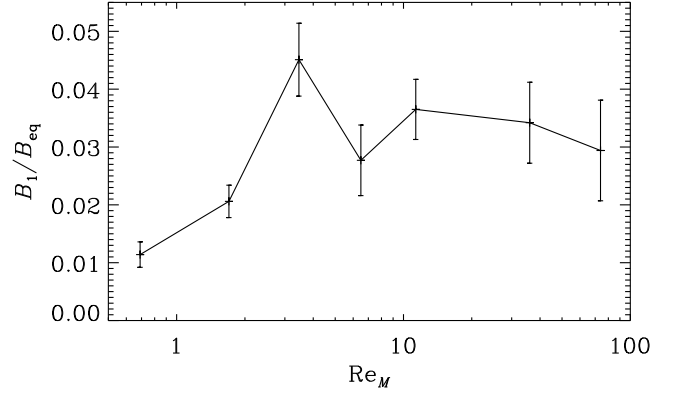


FIG. 2.— Dependence of  $B_1/B_{\text{eq}}$  (averaged over  $2 \leq k_1 z \leq 3$ ) on  $\text{Re}_M$  for  $B_0/B_{\text{eq}0} = 0.05$ .

to the top at  $k_1 z = \pi$ . (Note that  $B_1$  does not include the imposed field  $B_0$  at  $k = 0$ .)

The simulations are performed with the PENCIL CODE<sup>1</sup>, which uses sixth-order explicit finite differences in space and a third-order accurate time stepping method. We use numerical resolutions of  $128^3$  and  $256^3$  mesh points when  $L_x = L_y = L_z$ , and  $1024 \times 128^2$  when  $L_x = 8L_y = 8L_z$ . To capture mean-field effects on the slower turbulent-diffusive time scale, which is  $\tau_{\text{td}}/\tau_{\text{to}} = 3k_f^2/k_1^2$  times slower than the dynamical time scale, we perform simulations for several thousand turnover times.

### 3. RESULTS

The NEMPI phenomenon is already quite pronounced at intermediate values of  $\text{Re}_M \gtrsim 3$ ; see Fig. 1, where we show  $B_y$  averaged over  $y$  and  $\Delta t \approx 80\tau_{\text{to}}$  at selected times during the first 2000 turnover times. The  $\text{Re}_M$  dependence of  $B_1/B_{\text{eq}}$  is shown in Fig. 2. The  $\text{Re}_M$  dependence is relatively weak, although it becomes less certain for larger values, because of the long run times required and extended transients.

The case  $\text{Re}_M = 6$  shows strong similarities to what has previously been seen in mean-field simulations. During the first 500 turnover times, flux concentrations form first near the surface, but the location of the peak magnetic field moves then gradually downward. This phenomenon is a direct consequence of the negative effective magnetic pressure, making such structures heavier than their surroundings. Their shape resembles that of a falling ‘potato sack’ and has now been

<sup>1</sup> <http://pencil-code.googlecode.com>

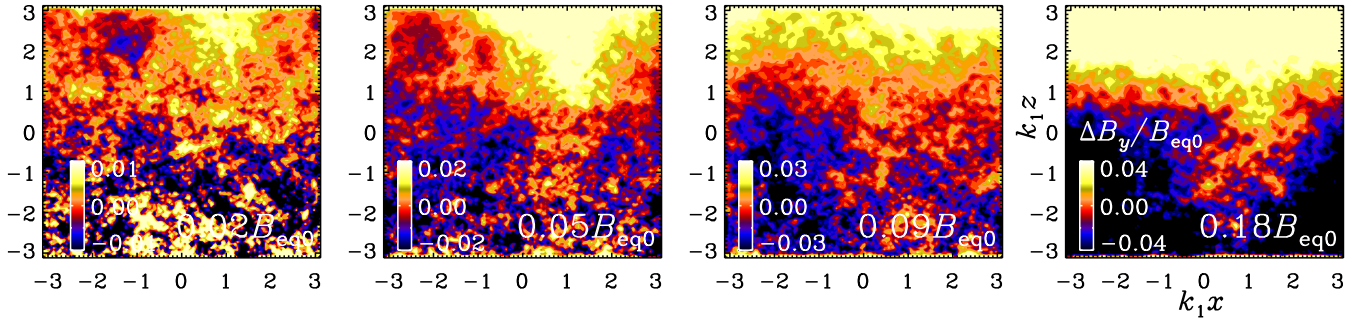


FIG. 3.—  $\Delta \bar{B}_y/B_{eq0}$  in the  $xz$  plane for  $\text{Re}_M = 36$  and  $B_0/B_{eq0} = 0.02, 0.05, 0.09$ , and  $0.18$ .

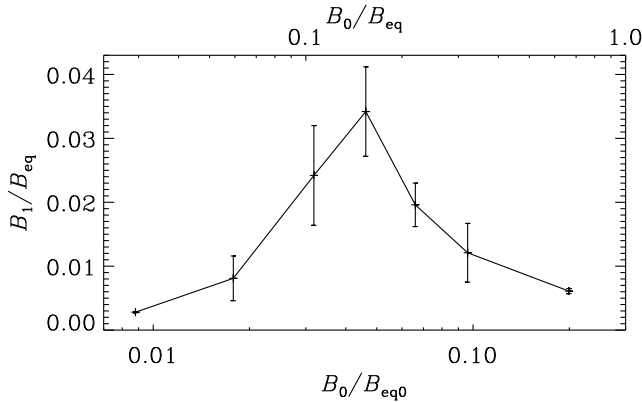


FIG. 4.— Bifurcation diagram showing  $B_1/B_{eq}$  versus  $B_0/B_{eq0}$  (and versus  $B_0/B_{eq}$  on the upper abscissa) for  $\text{Re}_M = 36$ .

seen in numerous mean-field calculations during the nonlinear stage of NEMPI (Brandenburg et al. 2010, 2011; Käpylä et al. 2011). We checked that also in this case with  $\text{Re}_M = 6$  the effective magnetic pressure is negative for  $0 \leq \bar{B} \lesssim 0.4B_{eq}$ .

As expected from theory and mean-field calculations, NEMPI is only excited in a certain range of field strengths. Indeed, only for intermediate values of  $B_0/B_{eq0}$  between 0.02 and 0.2 do we see clear evidence that the magnetic field gets concentrated into large-scale structures. This is shown in Fig. 3, where we see  $B_y$ , again averaged over  $y$  and  $\Delta t \approx 800\tau_{to}$ , during a time interval in which the field is statistically steady. The clearest flux structure formations are seen for  $B_0/B_{eq0} \approx 0.05$ . However, even for this case the magnetic field concentrations are barely visible in a single snapshot. This has been one of the reasons why NEMPI has not been noticed before in DNS. An additional handicap was that earlier simulations of Brandenburg et al. (2010, 2011) used a smaller scale separation ratio of only 5, even though it is still sufficient for determining the governing mean-field coefficients and allows one to reach larger values of  $\text{Re}_M$ .

In Fig. 4 we plot  $B_1/B_{eq}$  as a function of  $B_0/B_{eq0}$ , showing a peak at  $B_0/B_{eq0} \approx 0.05$ . The fact that large-scale flux concentrations develop only for a certain range of imposed field strengths supports our interpretation that they are caused by NEMPI and not, for example, by some unknown type of dynamo mechanism. In all these cases the magnetic field grows rapidly and reaches a saturation field strength that is independent of the imposed field provided  $\text{Re}_M \geq 35$ . This suggests that this field is produced by small-scale dynamo action and not just by field line tangling. Another piece of evidence of the physical reality of NEMPI is shown

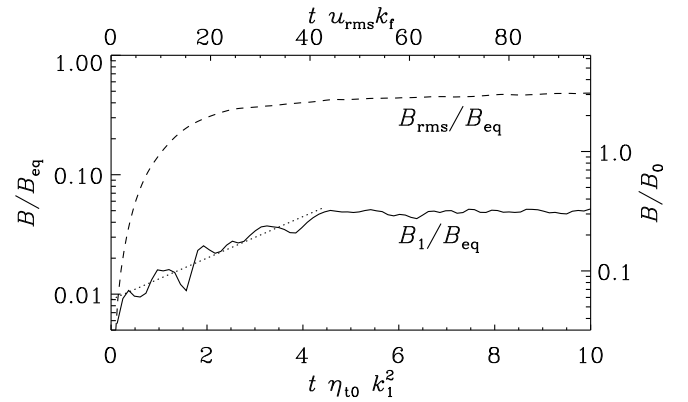


FIG. 5.— Slow exponential growth of the mean magnetic field in  $2 \leq k_1 z \leq 3$  for  $B_0/B_{eq0} = 0.05$ , corresponding to  $B_0/B_{eq} = 0.16$ , for  $\text{Re}_M = 36$  (solid line). The growth rate is  $\approx 0.4\eta_{t0}k_1^2$  (dotted line). Note that the total rms field,  $B_{rms}/B_{eq}$  (dotted line) saturates much faster, as indicated by upper abscissa.

in Fig. 5, where we see that  $B_1$  does indeed increase exponentially for the first 2000 turnover times, corresponding to about  $3\tau_{td}$ . The growth rate is  $\approx 0.4\eta_{t0}k_1^2$ , which is much less than  $\tau_{to}^{-1}$ , but entirely compatible with mean-field calculations (Käpylä et al. 2011).

Again, in agreement with earlier work (e.g., Fig. 14 of Käpylä et al. 2011), the most unstable mode has a wavelength comparable to the depth of the domain of  $\approx 6H_\rho$ ; see Fig. 6, where we compare cross-sections of  $\langle \Delta B_y \rangle_{yt}/B_{eq}$  for a calculation with  $B_0/B_{eq0} = 0.05$  and  $\text{Re}_M = 36$ , but an  $x$  extent of  $16\pi/k_1$ . The large-scale flux concentrations have an amplitude of only  $\approx 0.1B_{eq}$  and are therefore not seen in single snapshots, where the field reaches peak strengths comparable to  $B_{eq}$ . Furthermore, as for any linear instability, the flux concentrations form a repetitive pattern, and are in that sense similar to flux concentrations seen in the calculations of Kitchatinov & Mazur (1988) that were based on the magnetic suppression of the convective heat flux. However, there are indications that at larger values of  $\text{Re}_M$ , flux concentrations occur more rarely, which might be more realistic in view of astrophysical applications.

#### 4. CONCLUSIONS

The present simulations have, for the first time, demonstrated conclusively that the negative effective magnetic pressure instability can operate in hydromagnetic turbulence under proper conditions, namely strong stratification, sufficient scale separation (between the size of the domain and the forcing scale), and a mean field in an optimal range (in our simu-

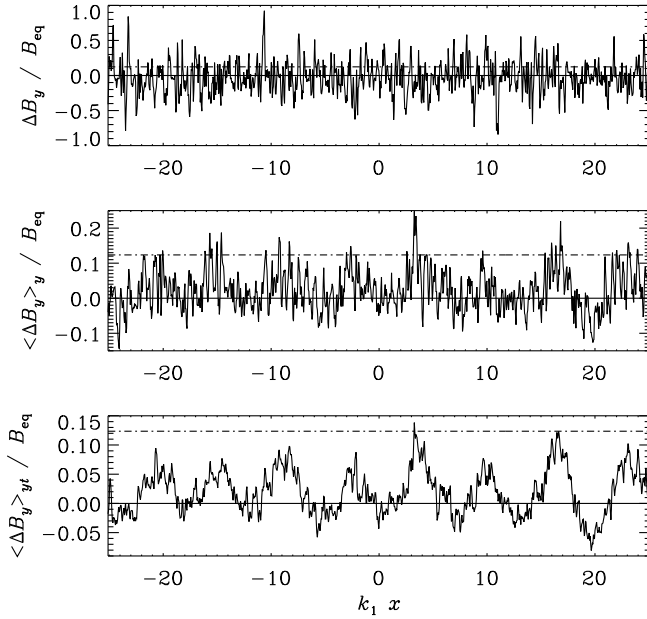


FIG. 6.—  $x$  dependence of the field for an elongated box ( $1024 \times 128^2$  mesh points) with  $\text{Re}_M = 36$  at  $k_1 z = 2$  showing  $\Delta B_y / B_{\text{eq}}$  at  $y = 0$  (top panel), its  $y$  average  $\langle \Delta B_y \rangle_y / B_{\text{eq}}$  (middle panel), as well as an additional time average  $\langle \Delta B_y \rangle_{yt} / B_{\text{eq}}$  (bottom panel) covering about 80 turnover times. The dash-dotted line gives the level of the imposed field.

lations  $\approx 0.15 B_{\text{eq}}$ ; see Fig. 4). This instability has so far been seen only in mean-field simulations.

Let us now ask whether this instability alone can describe the formation of active regions at the solar surface. Clearly the flux concentration we observe are not strong enough to be noticeable without averaging. But the active regions in the Sun are prominent enough to be visible without averaging. This suggests that there may be additional mechanisms at work. One such possibility is related to the magnetic suppression of the convective heat flux that has been invoked to explaining the formation of sunspots (Kitchatinov & Mazur 1988). Furthermore, simulations of convection with an imposed vertical field have suggested a segregation into magnetized and unmagnetized regions (Tao et al. 1998; Kitiashvili et al. 2010). In these examples, flux concentrations appear strong enough to be noticeable even without averaging.

Our work has established a close link between what can be expected from mean-field studies and what actually happens in DNS. This correspondence is particularly important because DNS cannot reach solar parameters in any conceivable future. Hence a deeper understanding of the solar convection can only emerge by studying mean-field models on one hand and to determine turbulent mean-field coefficients from simulations on the other hand. This concerns not only the dependence of the mean field coefficients on parameters such as magnetic Reynolds and Prandtl numbers and the scale separation ratio, but also details of the source of turbulence. In particular, it has already been shown that the negative effective magnetic pressure effect is not unique to forced turbulence, but it occurs also in turbulent convection Käpylä et al. (2011). It should therefore be emphasized that the present work has demonstrated the predictive power of mean-field theory at an advanced level where the second order correlation approximation fails (Rüdiger et al. 2011) and where the spectral  $\tau$  approach (Rogachevskii & Kleeorin 2007) has proven useful.

More work using mean-field models is needed to elucidate details of the mechanism of NEMPI. For example, naive thinking suggests that the onset of NEMPI should occur at the depth where the effective magnetic pressure is minimum, but both mean field models and DNS show that this is not the case. At least at early times, NEMPI appears most pronounced at the top of the domain, while the effective magnetic pressure is most negative at the bottom. On the other hand, the instability is a global one and local considerations such as these are not always meaningful. Another question is what happens when the imposed field is replaced by a dynamo-generated one. In that case, the turbulence may be helical and new terms involving current density can occur in the expression for the mean-field stress. Again, such possibilities are best studied using first the mean-field approach.

We acknowledge the NORDITA dynamo programs of 2009 and 2011 for providing a stimulating scientific atmosphere. Computing resources provided by the Swedish National Allocations Committee at the Center for Parallel Computers at the Royal Institute of Technology in Stockholm and the High Performance Computing Center North in Umeå. This work was supported in part by the European Research Council under the AstroDyn Research Project No. 227952.

## REFERENCES

- Brandenburg, A., Kleeorin, N., & Rogachevskii, I. 2010, *Astron. Nachr.*, 331, 5
- Brandenburg, A., Kemel, K., Kleeorin, N., & Rogachevskii, I. 2011, *ApJ*, submitted, arXiv:1107.2752
- Brandenburg, A., & Subramanian, K. 2005, *Phys. Rep.*, 417, 1
- Jiang, J., & Wang, J. X. 2007, *MNRAS*, 377, 711
- Käpylä, P. J., Brandenburg, A., Kleeorin, N., Mantere, M. J., & Rogachevskii, I. 2011, *MNRAS*, submitted, arXiv:1105.5785
- Käpylä, P. J., Korpi, M. J. & Brandenburg, A. 2009, *ApJ*, 697, 1153
- Kitchatinov, L.L., & Mazur, M.V. 2000, *Solar Phys.*, 191, 325
- Kitiashvili, I. N., Kosovichev, A. G., Wray, A. A., & Mansour, N. N. 2010, *ApJ*, 719, 307
- Kemel, K., Brandenburg, A., Kleeorin, N., & Rogachevskii, I. 2011, *Astron. Nachr.*, submitted, arXiv:1107.2752
- Kleeorin, N., Mond, M., & Rogachevskii, I. 1996, *A&A*, 307, 293
- Kleeorin, N., & Rogachevskii, I. 1994, *Phys. Rev. E*, 50, 2716
- Kleeorin, N.I., Rogachevskii, I.V., & Ruzmaikin, A.A. 1990, *Sov. Phys. JETP*, 70, 878
- Krause, F., & Rädler, K.-H. 1980, *Mean-field magnetohydrodynamics and dynamo theory* (Pergamon Press, Oxford)
- Moffatt, H.K. 1978, *Magnetic field generation in electrically conducting fluids* (Cambridge University Press, Cambridge)
- Parker, E.N. 1979, *Cosmical magnetic fields* (Oxford University Press, New York)
- Rädler, K.-H. 1974, *Astron. Nachr.*, 295, 265
- Rüdiger, G. 1974, *Astron. Nachr.*, 295, 275
- Rüdiger, G., Tuominen, I., Krause, F., Virtanen, H. 1986, *A&A*, 166, 306
- Rüdiger, G., Kitchatinov, L. L., & Schultz, M., 2011, *A&A*, submitted
- Rogachevskii, I., & Kleeorin, N. 2007, *Phys. Rev. E*, 76, 056307
- Stenflo, J. O., & Vogel, M. 1986, *Nature*, 319, 285
- Tao, L., Weiss, N. O., Brownjohn, D. P., & Proctor, M. R. E. 1998, *ApJ*, 496, L39